Electronic Supplementary Information for…

Mechanisms and Energetics for N-Glycosidic Bond Cleavage of Protonated Adenine Nucleosides: N3 Protonation Induces Base Rotation and Enhances N-Glycosidic Bond Stability

R. R. Wu and M. T. Rodgers*
Department of Chemistry, Wayne State University, Detroit, Michigan 48202, United States

Data Handling. Ion intensities are converted to absolute cross sections as described previously using a Beer's law analysis.[1] Due to the errors in the pressure measurement and uncertainties in the length of the interaction region, uncertainties in the cross-section magnitudes are ~±20%, whereas the relative uncertainties are ~ ±5%.

Ion kinetic energies in the laboratory frame are converted to energies in the center-of-mass frame, E_{CM}, using the formula, $E_{CM} = E_{lab}\, m/(m+M)$, where M and m are the masses of the ionic and neutral reactants, respectively. The absolute zero and distribution of the ion kinetic energies are determined using the octopole ion guide as a retarding potential analyzer as previously described.1 The distribution of ion kinetic energies is nearly Gaussian with a full width at half-maximum (fwhm) between 0.2 and 0.5 eV (lab) for these experiments. The uncertainty in the absolute energy scale is ±0.05 eV (lab).

The effects of multiple collisions can significantly influence the shape of CID cross sections,[2] even when the pressure of Xe is kept low. Pressure-dependent studies of all cross sections are measured. Cross sections are extrapolated to zero pressure2 of the Xe reactant to provide data that are rigorously the result of single collision conditions, and thus provide reliable thermochemistry.

Thermochemical Analysis. The parameters of eq 1 are defined as follows: σ_0 is an energy independent scaling factor, E is the relative translational energy of the reactants, E_0 is the threshold for reaction of the ground electronic and ro-vibrational state, E_i is the excitation energy of each state, and n is an adjustable parameter that describes the efficiency of kinetic to internal energy transfer.[3] τ is the experimental time available for dissociation, and k is the unimolecular dissociation rate constant. ΔE is the energy that remains in translation after collision between the reactants. $E + E_i - \Delta E$ is the internal energy of the energized molecule after the collision. The indices j refer to the individual dissociation channels, and k_j is the unimolecular rate constant for dissociation channel j ($\Sigma k_j = k_{tot}$). The scaling factors, $\sigma_{0,j}$, are ideally the same for all product channels. However, independent scaling was required to reproduce the data with high fidelity. The summation is over the ro-vibrational states of the reactant ions, $[dAdo+H]^+$ and $[Ado+H]^+$, where g_i is the population of those state ($\sum g_i = 1$). Because the $[dAdo+H]^+$ and $[Ado+H]^+$ ions possess many low-frequency vibrational modes, the populations of excited vibrational modes are not negligible at 298 K. Thus, the internal energy of the reactant ion contributes significantly to the reaction threshold (See Tables S1 and S2 of the Supporting Information). Whether the dissociation of $[dAdo+H]^+$ and $[Ado+H]^+$ occurs within the time scale of the experiments, ~10^{-4} s, must be taken into account in the thermochemical analysis

procedures to ensure extraction of accurate energetics. Therefore, Rice-Ramsperger-Kassel-Marcus (RRKM) theory is included as described in detail elsewhere.[4,5] Sets of ro-vibrational frequencies appropriate for the energized reactants and the transition states (TSs) leading to dissociation are required to properly analyze the threshold energies. For the activated dissociation processes studied here, the tight transition states (TTSs) associated with the pathways for N-glycosidic bond cleavage are explicitly modeled theoretically to determine appropriate molecular parameters for the thermochemical analysis of the experimental data. Before comparison to the experimental data, eq 1 is convoluted with the kinetic energy distributions of the $[dAdo+H]^+$ or $[Ado+H]^+$ and Xe reactants, and a nonlinear least-squares analysis of the data is performed to give optimized values for the parameters, σ_0, E_0, and n.

The density of ro-vibrational states[6–8] is evaluated using the Beyer-Swinehart algorithm and the relative populations, g_i, are calculated for a Maxwell-Boltzmann distribution at 298 K, the internal temperature of the reactants. The average internal energies at 298 K of the reactant ions, $[dAdo+H]^+$ and $[Ado+H]^+$, TSs and dissociation products are also given in Tables S1 and S2. The errors in the measured thresholds are estimated from the range of values determined for the zero-pressure-extrapolated data sets, ± 10% variations associated with uncertainties in the vibrational frequencies (prescaled by 0.99), and the error in the absolute energy scale, ± 0.05 eV (lab). For analyses that include the RRKM lifetime analysis, the uncertainties in the measured thresholds also include the effects of increasing and decreasing the time assumed available for dissociation by a factor of 2.

Details of the Potential Energy Surface Scans. All relaxed PES scans are performed at the B3LYP/6-31G(d) level of theory. The PESs for glycosidic bond cleavage/elongation are first scanned at a step size of 0.05 Å, typically with ~45−60 steps. The initial TS guesses for TS_1 are selected among the structures along these PESs, typically the least stable species computed when the PES scan is smooth. After TS and IRC calculations are performed to determine the optimized structure and to establish the appropriate Int_1s, the PESs scans on the C2'-H or C5'-H transfer of the Int_1s are also performed at a step size of 0.05 Å, typically with ~15−65 steps. The initial TS guesses for TS_2 are again selected among the structures computed along the PESs for C2'-H or C5'-H transfer. The initial TS guess for TS_n of $[Ado+H]^+$ is generated by scanning the proton transfer between N3 of adenine and O4 of the sugar moiety of Int_2 at a step size of 0.05 Å with 15 steps.

N-Glycosidic Bond Cleavage of N3 Protonated $[dAdo+H]^+$. The calculated PESs for N-glycosidic bond cleavage of $[dAdo+H]^+$ resulting in elimination of $[Ade+H]^+$ is shown in Figure 3a. In the ground-state conformer of $[dAdo+H]^+$, the glycosidic bond is 1.465 Å long. In the first step, the glycosidic bond elongates to 3.174 Å. Glycosidic bond lengthening is accompanied by rotation of the departing N3 protonated adenine moiety such that the ∠C4N9C1'C2' dihedral angle increases from −72.0° to −133.0° to facilitate interaction with the C2' hydrogen atom. The N3–H^+···O5' hydrogen bond is maintained as the adenine residue departs from the sugar leading to the first TS, TS_1. The relative energy difference between the ground-state conformation of $[dAdo+H]^+$ and TS_1 determines the first activation barrier. Rotation of the 5'-hydroxymethyl substituent along with further rotation of the nucleobase enables a second hydrogen-bonding interaction between N9 and the 5'-hydroxyl hydrogen atoms, leading

to a stable oxacarbenium ion intermediate, Int_1. Further rotation of the adenine moiety better aligns the N9 atom with H2' of the charged sugar and facilitates proton transfer from C2' of the sugar to N9 of adenine, forming a proton bound dimer between the nucleobase and sugar that leads to the formation of TS_2. The relative energy difference between the ground-state conformation of $[dAdo+H]^+$ and TS_2 determines the second activation barrier. As H2' is transferred to N9, forming protonated adenine, the electron density adjusts to form a double bond between C1' and C2', leading to a planar neutral sugar. The N3 protonated adenine and the neutral planar sugar moieties are stabilized by a N3–H^+···O5' hydrogen-bonding interaction and a N9–H···C2' noncanonical hydrogen-bonding interaction, forming a second stable intermediate, Int_2. Cleavage of these noncovalent interactions leads to smooth dissociation into the products, protonated adenine and the neutral 2'-deoxyribose sugar moiety.

The calculated PESs for N-glycosidic bond cleavage of $[dAdo+H]^+$ resulting in elimination of Ade is shown in Figure 3b. TS_1 along the PES for elimination of $[Ade+H]^+$ is also predicted as the glycosidic bond elongation step for loss of Ade pathway, which contrasts to that found for protonated cytosine and guanine nucleosides.[9,10] Due to the lack of strong intramolecular stabilization in these systems, as the glycosidic bond elongates, the overall structure is relatively flexible, such that a more stable TS, TS_n, involving a different orientation and relative position of the nucleobase to the sugar is accessed along the neutral nucleobase loss pathway. To eliminate neutral adenine, by breaking the strong hydrogen-bonding stabilizations in Int_1, the oxacarbenium intermediate smoothly dissociates into the positively charged nonplanar 2'-deoxyribose sugar and a noncanonical minor tautomer of neutral adenine.

N-Glycosidic Bond Cleavage of N3 Protonated $[Ado+H]^+$. The calculated PESs for N-glycosidic bond cleavage to produce $[Ade+H]^+$ and $[Ado-Ade+H]^+$ from N3 protonated $[Ado+H]^+$ are shown in Figure 4. In the ground-state conformer of $[Ado+H]^+$, the glycosidic bond is 1.459 Å long. In the first step, the glycosidic bond elongates to 3.201 Å. Glycosidic bond lengthening is again accompanied by rotation of the departing N3 protonated adenine moiety such that the ∠C4N9C1'C2' dihedral angle increases from −71.8° to −135.5° to facilitate interaction with the C2' hydrogen atom. The N3–H^+···O5' hydrogen bond is maintained as the adenine residue departs from the sugar leading to the first TS, TS_1^+. The relative energy difference between ground-state conformer of $[Ado+H]^+$ and TS_1^+ determines the first activation barrier. Rotation of the 5'-hydroxymethyl substituent and the nucleobase enables a second hydrogen-bonding interaction between the N9 and 5'-hydroxyl hydrogen atoms, leading to a stable oxocarbenium ion intermediate, Int_1. Instead of the nucleobase approaching the C2' hydrogen atom, facilitating proton transfer from C2' to N9, the 5'-hydroxyl hydrogen atom approaches N9, while a bond is formed between C1' and O5', leading to TS_2, which both levels of theory predict is lower in energy than TS_1. Transfer of the 5'-hydroxyl hydrogen atom to N9, produces Int_2, which is stabilized by N9–H···O5' and N3–H^+···O4' hydrogen-bonding interactions between protonated adenine and the double-ring sugar. Noncovalent cleavage of these two hydrogen-bonding interactions, produces the dissociation products, protonated adenine and the neutral double-ring sugar. Production of $[Ado-Ade+H]^+$ and neutral Ade is achieved by transfer of the excess proton from N3 to O1' in Int_2

passing through TS_n and resulting in Int_n, which is stabilized by the O4'–H···N3 and N9–H···O5' hydrogen-bonding interactions. The cleavage of these interactions produces the canonical neutral Ade moiety. The bond between C1' and O4' breaks and produces a six membered ring. Because the ion must go by Int_n to produce $[Ado\text{-}Ade+H]^+$ and neutral Ade, the activation barriers of TS_1 and TS_2 must first be overcome. TS_1, TS_2 and TS_n all lie below the dissociation asymptote, but the energy difference between TS_1 and the dissociation asymptote is relatively small. Therefore, TS_1 may still influence the rate of dissociation.

Conversion from 0 to 298 K. Standard formulas (assuming harmonic oscillator and rigid rotor models) and the vibrational and rotational constants determined for the B3LYP/6-311+G(d,p) optimized geometries of N3 protonated $[dAdo+H]^+$ and $[Ado+H]^+$, rate-limiting TSs and dissociation products for the N-glycosidic bond cleavage pathways of these systems, which are given in Tables S1 and S3 of the Electronic Supplementary Information, are used to convert the 0 K AEs and ΔH_{rxn}s determined from the threshold analyses to 298 K enthalpies and free energies. Table S10 lists 0 and 298 K enthalpies, free energies, and enthalpic and entropic corrections for N-glycosidic bond cleavage of N3 protonated $[dAdo+H]^+$ and $[Ado+H]^+$ experimentally determined. Uncertainties in the enthalpic and entropic corrections are calculated assuming that a ± 10% variation in all vibrationl frequencies, and additionally a ±50% variation in the frequencies below 300 cm^{-1} provide a good estimate of the uncertainty in these molecular parameters.

The relative energetics along the PESs for glycosidic bond cleavage to produce the protonated nucleobase, reaction (2), from both N3 and N1 protonated $[dAdo+H]^+$ and $[Ado+H]^+$ in solution are calculated using a polarizable continuum model (PCM). The results are summarized in Tables S11 and S12, respectively. Comparison of the results of Tables S11 and S12 to those in vacuo summarized in Tables 1 and 2, respectively, indicate that for both $[dAdo+H]^+$ and $[Ado+H]^+$, except for the final products, the solvent does not significantly influence the relative energetics along the PESs of the N1 protonated species, but lowers the energies of the rate-determining TS, TS_1 (AEs) along the PESs of the N3 protonated species by ~30 kJ/mol. Thus, N-glycosidic bond cleavage arising from N3 protonated conformers becomes even more favorable than that from N1 protonated species in solution.

References

1 K. M. Ervin and P. B. Armentrout, *J. Chem. Phys.*, 1985, **83**, 166.
2 N. F. Dalleska, K. Honma, L. S. Sunderlin and P. B. Armentrout, *J. Am. Chem. Soc.*, 1994, **116**, 3519.
3 F. Muntean, and P. B. Armentrout, *J. Chem. Phys*., 2001, **115**, 1213.
4 M. T. Rodgers, K. M. Ervin and P. B. Armentrout, *J. Chem. Phys.*, 1997, **106**, 4499.
5 F. A. Khan, D. E. Clemmer, R. H. Schultz and P. B. Armentrout, *J. Phys. Chem.*, 1993, **97**, 7978.
6 T. S. Beyer and D. F. Swinehart, *Commun. ACM* , 1973, **16**, 379.
7 S. E. Stein and B. S. Rabinovitch, *J. Chem. Phys.*, 1973, **58**, 2438.
8 S. E. Stein and B. S. Rabinovitch, *Chem. Phys. Lett.*, 1977, **49**, 183.
9 R. R. Wu and M. T. Rodgers, Anal. Chem., 2016, submitted.
10 R. R. Wu, Y. Chen and M. T. Rodgers, Phys. Chem. Chem. Phys., 2016, **18**, 2968.

Table S1. Vibrational Frequencies and Average Internal Energies of N3 Protonated Ground-State Conformations of $[dAdo+H]^+$ and $[Ado+H]^+$, Transition States, and Products Associated with their N-Glycosidic Bond Cleavage Reactions.

Species	E_{vib}, eV[a]	Vibrational frequencies, cm^{-1}[b]
$[dAdo+H]^+$	0.39 (0.04)	46, 59, 79, 116, 135, 149, 159, 198, 234, 256, 282, 292, 304, 334, 354, 366, 405, 449, 479, 495, 526, 535, 596, 602 623, 648, 656, 673, 722, 735, 771, 813, 858, 860, 875, 885, 903, 916, 943, 958, 971, 986, 1007,1045, 1067, 1080, 1095, 1112, 1171, 1185, 1200, 1206, 1218, 1236, 1261, 1266, 1273, 1311, 1325, 1329, 1347, 1367, 1377, 1400, 1407, 1417, 1425, 1465, 1472, 1490, 1499, 1522, 1552, 1621, 1647, 1671, 3012, 3021, 3025, 3039, 3042, 3061, 3093, 3157, 3168, 3214, 3536, 3660, 3791, 3800
$[dAdo+H]^+\_TS_1$	0.42 (0.04)	22, 38, 51, 67, 84, 119, 139, 163, 169, 201, 224 ,257, 279, 289, 307, 365, 385, 388, 425, 511, 523, 533, 581, 609, 627, 663, 671, 676, 713, 725, 748, 764, 783, 825, 863, 889, 903, 922, 925, 950, 958, 965, 987, 991, 1043, 1090, 1104, 1127, 1145, 1179, 1186, 1205, 1233, 1250, 1263, 1266, 1300, 1305, 1310, 1345, 1348, 1376, 1377, 1390, 1419, 1428, 1436, 1464, 1478, 1488, 1517, 1561, 1603, 1615, 1662, 2583, 3012, 3051, 3057, 3066, 3091, 3156, 3157, 3183, 3460, 3551, 3679, 3788, 3802
$[dAdo-Ade+H]^+$	0.19 (0.02)	98, 140, 174, 217, 283, 320, 358, 376, 412, 615, 657, 737, 778, 833, 865, 928, 948, 968, 989, 1052, 1095, 1105, 1185, 1195, 1222, 1236, 1249, 1286, 1303, 1332, 1352, 1378, 1420, 1433, 1489, 1600, 2986, 2990, 3033, 3057, 3064, 3119, 3135, 3790, 3798
Ade_noncanonical	0.17 (0.02)	148, 181, 228, 275, 293, 506, 521, 530, 556, 605, 636, 658, 682, 712, 757, 900, 905, 906, 941, 982, 1120, 1162, 1177, 1242, 1285, 1346, 1366, 1427, 1456, 1467, 1518, 1594, 1609, 1660, 3157, 3189, 3554, 3567, 3698
$[Ado+H]^+$	0.42 (0.04)	44, 54, 65, 110, 130, 141, 149, 192, 219, 233, 251, 265, 281, 296, 330, 335, 354, 379, 425, 481, 487, 511, 527, 535, 539, 597, 604, 624, 648, 672, 690, 715, 728, 771, 842, 859, 862, 865, 893, 904, 919, 954, 972, 986, 1032, 1052, 1066, 1069, 1088, 1109, 1132, 1165, 1181, 1194, 1213, 1235, 1248, 1261, 1265, 1267, 1295, 1321, 1331, 1342, 1366, 1378, 1400, 1404, 1412, 1418, 1426, 1472, 1490, 1499, 1523, 1551, 1622, 1644, 1671, 3007, 3016, 3030, 3044, 3052, 3056, 3168, 3197, 3220, 3536, 3660, 3704, 3797, 3812
$[Ado+H]^+\_TS_1$	0.45 (0.06)	24, 32, 41, 61, 75, 77, 115, 128, 153, 172, 187, 202, 217, 272, 281, 304, 339, 365, 381, 443, 478, 511, 523, 533, 549, 581, 609, 621, 663, 674, 687, 710, 714, 737, 752, 773, 846, 866, 896, 904, 914, 924, 950, 958, 987, 1020, 1031, 1084, 1103, 1125, 1140, 1157, 1183, 1200, 1223, 1225, 1248, 1257, 1268, 1290, 1302, 1311, 1344, 1350, 1360, 1375, 1409, 1419, 1424, 1436, 1464, 1476, 1486, 1516, 1554, 1600, 1615, 1662, 2504, 3013, 3056, 3075, 3091, 3149, 3158, 3190, 3482, 3551, 3679, 3721, 3803, 3806
$[Ado-Ade+H]^+$	0.19 (0.03)	65, 153, 209, 248, 300, 325, 353, 395, 430, 473, 487, 573, 578, 682, 707, 768, 812, 892, 927, 984, 1021, 1042, 1082, 1125, 1146, 1188, 1206, 1229, 1246, 1289, 1309, 1336, 1340, 1362, 1373, 1389, 1413, 1463, 1606, 2874, 3003, 3056, 3068, 3114, 3151, 3689, 3748, 3792
Ade_canonical	0.17 (0.02)	52, 163, 214, 274, 295, 511, 515, 526, 534, 569, 612, 661, 678, 718, 801, 843, 891, 935, 966, 998, 1068, 1131, 1230, 1254, 1314, 1343, 1350, 1400, 1418, 1486, 1499, 1592, 1618, 1640, 3136, 3208, 3573, 3612, 3704

[a]Present results, uncertainties are listed in parentheses. [b]Vibrational frequencies scaled by 0.99 obtained from vibrational analysis of the geometry optimized structures determined at the B3LYP/6-311+G(d,p) level of theory.

Table S2. Vibrational Frequencies and Average Internal Energies of N1 Protonated Conformations of $[dAdo+H]^+$ and $[Ado+H]^+$, Transition States, and Products Associated with their N-Glycosidic Bond Cleavage Reactions.

Species	E_{vib}, eV[a]	Vibrational frequencies, cm^{-1}[b]
$[dAdo+H]^+$	0.40 (0.04)	31, 54, 60, 102, 131, 138, 165, 210, 218, 242, 262, 273, 294, 306, 316, 327, 356, 386, 445, 504, 514, 557, 566, 615, 625, 631, 656, 659, 683, 727, 755, 773, 799, 856, 872, 899, 911, 912, 932, 946, 973, 986, 999, 1052, 1063, 1083, 1088, 1100, 1123, 1176, 1199, 1209, 1217, 1222, 1255, 1270, 1284, 1314, 1328, 1340, 1352, 1365, 1369, 1403, 1415, 1425, 1430, 1433, 1464, 1469, 1490, 1504, 1567, 1613, 1631, 1696, 2987, 3027, 3032, 3046, 3047, 3052, 3097, 3176, 3199, 3536, 3543, 3656, 3795, 3804
$[dAdo+H]^+\_TS_1$	0.43(0.04)	20, 22, 48, 58, 86, 112, 121, 136, 164, 171, 218, 242, 266, 277, 279, 308, 365, 380, 437, 470, 516, 537, 557, 602, 611, 622, 628, 677, 677, 713, 729, 751, 780, 835, 874, 874, 902, 916, 933, 950, 965, 979, 983, 1003, 1054, 1089, 1107, 1112, 1157, 1177, 1180, 1192, 1223, 1241, 1258, 1267, 1283, 1312, 1318, 1337, 1355, 1359, 1374, 1382, 1405, 1421, 1435, 1444, 1477, 1490, 1526, 1574, 1603, 1623, 1690, 2682, 2978, 3022, 3045, 3060, 3108, 3114, 3167, 3192, 3549, 3561, 3672, 3793, 3810
$[dAdo+H]^+\_TS_n$	0.43 (0.04)	18, 28, 40, 56, 83, 98, 136, 140, 163, 186, 219, 240, 255, 278, 280, 297, 366, 377, 416, 475, 514, 538, 558, 604, 612, 624, 629, 678, 690, 695, 714, 755, 782, 832, 861, 878, 901, 914, 925, 947, 957, 970, 984, 1004, 1047, 1085, 1102, 1109, 1156, 1174, 1176, 1188, 1223, 1248, 1257, 1263, 1287, 1319, 1321, 1334, 1357, 1360, 1375, 1384, 1404, 1420, 1434, 1446, 1476, 1489, 1528, 1574, 1604, 1624, 1689, 2965, 2980, 3028, 3049, 3058, 3094, 3111, 3166, 3191, 3549, 3560, 3671, 3793, 3810
$[dAdo-Ade+H]^+$	0.19 (0.02)	98, 140, 173, 214, 283, 320, 358, 376, 412, 615, 656, 737, 777, 833, 865, 928, 948, 968, 989, 1053, 1095, 1105, 1185, 1195, 1222, 1236, 1249, 1285, 1303, 1332, 1352, 1378, 1420, 1433, 1489, 1600, 2986, 2990, 3033, 3057, 3065, 3119, 3135, 3791, 3798
Ade_noncanonical	0.16 (0.02)	152, 213, 266, 273, 306, 506, 527, 536, 548, 586, 610, 627, 672, 711, 751, 864, 892, 923, 935, 1001, 1097, 1156, 1181, 1250, 1302, 1344, 1366, 1389, 1428, 1485, 1530, 1599, 1622, 1684, 3153, 3182, 3524, 3570, 3631
$[Ado+H]^+$	0.42 (0.04)	29, 49, 57, 88, 115, 133, 150, 201, 205, 231, 239, 258, 276, 292, 309, 315, 323, 338, 347, 427, 483, 505, 515, 536, 559, 569, 620, 626, 634, 657, 681, 685, 722, 745, 772, 831, 860, 886, 902, 910, 916, 935, 968, 984, 1030, 1041, 1067, 1073, 1095, 1103, 1120, 1130, 1178, 1183, 1202, 1221, 1248, 1254, 1277, 1281, 1305, 1329, 1334, 1352, 1363, 1371, 1402, 1406, 1415, 1427, 1431, 1435, 1466, 1490, 1506, 1568, 1614, 1632, 1696, 2982, 3026, 3034, 3040, 3048, 3071, 3176, 3207, 3537, 3544, 3657, 3710, 3804, 3813
$[Ado+H]^+\_TS_1$	0.47 (0.04)	21, 31, 51, 57, 76, 83, 119, 135, 152, 163, 179, 213, 221, 268, 278, 281, 288, 346, 359, 442, 469, 489, 515, 537, 553, 557, 602, 611, 619, 628, 677, 685, 713, 725, 753, 762, 853, 873, 895, 902, 916, 935, 951, 977, 984, 1029, 1041, 1087, 1105, 1111, 1138, 1157, 1178, 1182, 1199, 1229, 1245, 1254, 1260, 1287, 1306, 1318, 1336, 1357, 1362, 1373, 1404, 1412, 1413, 1433, 1443, 1478, 1489, 1526, 1568, 1602, 1624, 1690, 2673, 2971, 3019, 3086, 3109, 3139, 3166, 3192, 3548, 3561, 3670, 3711, 3810, 3811
$[Ado+H]^+\_TS_n$	0.47 (0.04)	21, 22, 37, 53, 71, 89, 133, 150, 156, 166, 182, 215, 221, 264, 277, 280, 288, 346, 355, 439, 474, 483, 514, 538, 554, 559, 604, 613, 630, 631, 678, 679, 714, 723, 759, 769, 840, 879, 897, 900, 914, 935, 947, 968, 985, 1020, 1043, 1085, 1097, 1108, 1128, 1156, 1176, 1178, 1195, 1226, 1251, 1253, 1257, 1291, 1304, 1320, 1333, 1358, 1359, 1375, 1395, 1403, 1412, 1434, 1447, 1475, 1490, 1529, 1569, 1604, 1624, 1688, 2978, 2997, 3015, 3028, 3083, 3110, 3166, 3192, 3549, 3560, 3671, 3705, 3810, 3813

Table S2. (cont'd.) Vibrational Frequencies and Average Internal Energies of N1 Protonated Conformations of $[dAdo+H]^+$ and $[Ado+H]^+$, Transition States, and Products Associated with their N-Glycosidic Bond Cleavage Reactions.

Species	E_{vib}, eV[a]	Vibrational frequencies, cm^{-1}[b]
$[Ado-Ade+H]^+$	0.22 (0.02)	88, 107, 160, 187, 221, 288, 316, 345, 353, 435, 488, 558, 607, 679, 735, 766, 840, 898, 944, 973, 1029, 1050, 1084, 1100, 1136, 1179, 1198, 1221, 1243, 1253, 1287, 1297, 1329, 1337, 1377, 1412, 1432, 1490, 1603, 2984, 3001, 3031, 3081, 3118, 3132, 3689, 3794, 3799
Ade_noncanonical	0.16 (0.02)	152, 213, 266, 273, 306, 506, 527, 536, 548, 586, 610, 627, 672, 711, 751, 864, 892, 923, 935, 1001, 1097, 1156, 1181, 1250, 1302, 1344, 1366, 1389, 1428, 1485, 1530, 1599, 1622, 1684, 3153, 3182, 3524, 3570, 3631

[a]Present results, uncertainties are listed in parentheses. [b]Vibrational frequencies scaled by 0.99 obtained from vibrational analysis of the geometry optimized structures determined at the B3LYP/6-311+G(d,p) level of theory.

Table S3. Rotational Constants of N3 Protonated $[dAdo+H]^+$ and $[Ado+H]^+$ and the Corresponding Tight Transition States for N-Glycosidic Bond Cleavage.

CID Products	Energized Molecule			Transition State	
	1-D[a]	2-D[b]		1-D[c]	2-D[c]
$[Ade+H]^+$ from $[dAdo+H]^+$	0.030	0.0085	TS_1	0.030	0.0066
$[dAdo-Ade+H]^+$	0.030	0.0085	TS_1	0.030	0.0066
$[Ade+H]^+$ from $[Ado+H]^+$	0.025	0.0080	TS_1	0.025	0.0062
$[Ado-Ade+H]^+$	0.025	0.0080	TS_1	0.025	0.0062

[a]Active external. [b]Inactive external. [c]Rotational constants of the transition state treated as free internal rotors.

Table S4. Rotational Constants of N1 Protonated $[dAdo+H]^+$ and $[Ado+H]^+$ and the Corresponding Tight and Phase Space Limit Transition States for N-Glycosidic Bond Cleavage.

CID Products	Energized Molecule			Transition State		
	1-D[a]	2-D[b]		1-D[c]	2-D[c]	2-D[d]
$[Ade+H]^+$ from $[dAdo+H]^+$	0.033	0.0073	TS_1	0.030	0.0061	-
$[dAdo-Ade+H]^+$	0.033	0.0073	TS_n	0.029	0.0061	-
			PSL	0.10, 0.077	0.058, 0.041	0.0016
$[Ade+H]^+$ from $[Ado+H]^+$	0.027	0.0070	TS_1	0.026	0.0061	-
$[Ado-Ade+H]^+$	0.027	0.0070	TS_n	0.025	0.0059	-
			PSL	0.085, 0.077	0.043, 0.041	0.0014

[a]Active external. [b]Inactive external. [c]Rotational constants of the transition state treated as free internal rotors. [d]Two-dimensional rotational constant of the TS at threshold, treated variantionally and statistically.

Table S5. Fragments Derived from Sequential Dissociation of $[dAdo\text{-}Ade+H]^+$ and $[Ado\text{-}Ade+H]^+$.

	m/z	Chemical Formula	Symbol[a]	Neutral Loss[b]
$[dAdo\text{-}Ade+H]^+$	99	$C_5H_7O_2^+$	▽	H_2O
m/z = 117	81	$C_5H_5O^+$	◇	$2H_2O$
$C_5H_9O_3^+$	67	$C_4H_3O^+$	△	H_2O, CH_4O
	55	$C_3H_3O^+$	○	$2H_2O$, C_2H_2
	41	C_2HO^+	□	H_2O, CH_4O, C_2H_2
$[Ado\text{-}Ade+H]^+$	115	$C_5H_7O_3^+$	▽	H_2O
m/z = 133	97	$C_5H_5O_2^+$	◇	$2H_2O$
$C_5H_9O_4^+$	83	$C_4H_3O_2^+$	△	H_2O, CH_4O
	71	$C_3H_3O_2^+$	○	$2H_2O$, C_2H_2
	53	C_3HO^+	□	H_2O, CH_4O, CH_2O
	41	C_2HO^+	☆	$2H_2O$, C_2H_2, CH_2O

[a]Symbols designations correspond to the CID product cross sections shown in Figure 2. [b]Proposed sequential neutral losses from the primary $[dAdo\text{-}Ade+H]^+$ and $[Ado\text{-}Ade+H]^+$ CID products.

Table S6. Fitting Parameters of Equation 1, Activation Energies and Reaction Enthalpies at 0 K, and Entropies of Activation at 1000 K of N3 Protonated $[dAdo+H]^+$ Obtained from Competitive Threshold Analyses for N-Glycosidic Bond Cleavage of $[dAdo+H]^+$[a]

Cross Section	TS	σ_0	n	E_0 (eV)	$\Delta S^{\ddagger}_{1000}$ (J mol^{-1} K^{-1})
$[Ade+H]^+$	TS_1	10.4 (0.5)	1.3 (0.1)	1.53 (0.05)	41 (1)
$[dAdo\text{-}Ade+H]^+$	TS_1	770 (150)	1.3 (0.1)	2.00 (0.05)	41 (1)
$[Ade+H]^+$	TS_1	9.0 (1.5)	1.6 (0.1)	1.49 (0.04)	41 (1)
$[dAdo\text{-}Ade+H]^+$	PSL	3.3 (0.7)	1.6 (0.1)	2.39 (0.06)	124 (4)
$[Ade+H]^+$	TS_1	10.7 (0.3)	1.3 (0.1)	1.53 (0.05)	41 (1)
$[dAdo\text{-}Ade+H]^+$	SW	670 (170)	1.3 (0.1)	2.00 (0.05)	124 (4)

[a]Uncertainties are listed in parentheses.

Table S7. Fitting Parameters of Equation 1, Activation Energies and Reaction Enthalpies at 0 K, and Entropies of Activation at 1000 K of N3 Protonated $[Ado+H]^+$ Obtained from Competitive Threshold Analyses for N-Glycosidic Bond Cleavage of $[Ado+H]^+$[a]

Cross Section	TS	σ_0	n	E_0 (eV)	$\Delta S^{\ddagger}_{1000}$ (J mol^{-1} K^{-1})
$[Ade+H]^+$	TS_1	24 (2)	1.3 (0.1)	1.70 (0.05)	53 (1)
$[dAdo\text{-}Ade+H]^+$	TS_1	170 (30)	1.3 (0.1)	2.02 (0.05)	53 (1)
$[Ade+H]^+$	TS_1	25 (1)	2.1 (0.1)	1.67 (0.05)	53 (1)
$[dAdo\text{-}Ade+H]^+$	PSL	1.1 (0.2)	2.1 (0.1)	2.32 (0.08)	122 (4)
$[Ade+H]^+$	TS_1	25 (5)	1.3 (0.2)	1.71 (0.06)	53 (1)
$[dAdo\text{-}Ade+H]^+$	SW	170 (40)	1.3 (0.2)	2.02 (0.05)	122 (4)

[a]Uncertainties are listed in parentheses.

Table S8. Fitting Parameters of Equation 1, Activation Energies and Reaction Enthalpies at 0 K, and Entropies of Activation at 1000 K of N1 Protonated $[dAdo+H]^+$ and $[Ado+H]^+$ Obtained from Competitive Threshold Analyses for N-Glycosidic Bond Cleavage of N1 Protonated $[dAdo+H]^+$ and $[Ado+H]^+$[a]

Cross Section	TS	σ_0	n	E_0 (eV)	$\Delta S^{\ddagger}_{1000}$ (J mol^{-1} K^{-1})
$[Ade+H]^+$ from $[dAdo+H]^+$	TS_1	10.5 (0.4)	1.4 (0.1)	1.53 (0.05)	42 (1)
$[dAdo-Ade+H]^+$	SW	8.7 (0.9)	1.4 (0.1)	2.36 (0.07)	102 (4)
$[Ade+H]^+$ from $[Ado+H]^+$	TS_1	17.9 (2.0)	1.8 (0.1)	1.55 (0.05)	39 (1)
$[Ado-Ade+H]^+$	SW	4.9 (1.3)	1.8 (0.1)	2.30 (0.07)	103 (4)

[a]Uncertainties are listed in parentheses.

Table S9. Activation Energies and Reaction Enthalpies for N-Glycosidic Bond Cleavage of N1 Protonated $[dAdo+H]^+$ and $[Ado+H]^+$ at 0 K in kJ/mol.[a]

CID Products	TCID[b]		B3LYP[c]		B3LYP-GD3BJ[d]		MP2[e]	
	AE	ΔH_{rxn}	AE	ΔH_{rxn}[f]	AE	ΔH_{rxn}[f]	AE	ΔH_{rxn}[f]
$[Ade+H]^+$ from $[dAdo+H]^+$	147.6 (4.8)	-	114.0	70.8	126.0	107.2	149.8	87.8
$[dAdo-Ade+H]^+$	-	227.7 (6.8)	110.9	204.0	123.5	230.4	147.6	223.9
$[Ade+H]^+$ from $[Ado+H]^+$	149.6 (4.8)	-	146.3	74.3	156.4	102.9	181.2	95.3
$[Ado-Ade+H]^+$	-	221.9 (6.8)	137.6	228.8	150.3	256.0	175.6	250.4
AEU[g]	4.8 (0.0)	6.8 (0.0)						
MAD[h]			18.5 (21.4)	15.3 (11.9)	14.2 (10.5)	18.4 (22.2)	16.9 (20.8)	16.2 (17.5)

[a]Present results, uncertainties are listed in parenthess. [b]TCID activation energies and reaction enthalpies obtained from competitive threshold analyses. [c]Calculated at B3LYP/6-311+G(2d,2p)//B3LYP/6-311+G(d,p) level of theory including ZPE correction. [d]Calculated at B3LYP-GD3BJ/6-311+G(2d,2p)//B3LYP/6-311+G(d,p) level of theory. [e]Calculated at MP2(full)/6-311+G(2d,2p)//B3LYP/6-311+G(d,p) level of theory including ZPE correction. [f]Also includes BSSE corrections. [g]Average experimental uncertainty (AEU). [h]The mean absolute deviation (MAD) between calculated and experimentally obtained AEs and ΔH_{rxn}s.

Table S10. Enthalpies and Free Energies for N-Glycosidic Bond Cleavage of $[dAdo+H]^+$ and $[Ado+H]^+$ at 0 and 298 K in kJ/mol.[a]

Reactant	CID Product	ΔH_0	ΔH_0[b]	ΔH_{298}-ΔH_0[b]	ΔH_{298}	ΔH_{298}[b]	$T\Delta S_{298}$[b]	ΔG_{298}	ΔG_{298}[b]
$[dAdo+H]^+$	$[Ade+H]^+$	147.6 (4.8)	146.8	5.4 (0.4)	153.0 (4.8)	152.2	12 (3.4)	141.0 (5.9)	140.2
	$[dAdo-Ade+H]^+$	193.0 (4.8)	188.4	5.4 (0.4)	198.4 (4.8)	193.8	12 (3.4)	186.4 (5.9)	181.8
$[Ado+H]^+$	$[Ade+H]^+$	164.0 (4.8)	172.3	6.3 (0.7)	170.3 (4.9)	178.6	15.4 (2.3)	154.9 (5.4)	163.2
	$[dAdo-Ade+H]^+$	194.9 (4.8)	189.7	6.3 (0.7)	201.2 (4.9)	196.0	15.4 (2.3)	185.8 (5.4)	180.6

[a]Present results, uncertainties are listed in parenthese. [b]Values from the theoretical calculations at the B3LYP/6-311+G(2d,2p) level of theory using the B3LYP/6-311+G(d,p) optimized geometries.

Table S11. Relative Energies (kJ/mol) of the Reactants, Transition States, Intermediates and Products for Producing $[Ade+H]^+$ from N3 Protonated $[dAdo+H]^+$ and $[Ado+H]^+$ with a Polarizable Continuum Model.

CID Channel		Relative Energies[a]		CID Channel		Relative Energies[a]	
		B3LYP	MP2			B3LYP	MP2
$[Ade+H]^+$	$[dAdo+H]^+$	**0.0**	**0.0**	$[Ade+H]^+$	$[Ado+H]^+$	**0.0**	**0.0**
	TS_1	117.6	158.4		TS_1	142.1	**184.0**
	Int_1	116.9	147.3		Int_1	140.7	172.0
	TS_2	**120.7**	**159.2**		TS_2	**145.6**	175.5
	Int_2	36.7	75.3		Int_2	24.9	39.2
	ΔH_{rxn} [b]	51.6	70.4		ΔH_{rxn} [b]	44.8	40.5

[a]B3LYP/6-311+G(2d,2p) and MP2/6-311+G(2d,2p) relative energies of B3LYP/6-311+G(d,p) optimized structures at 0 K including ZPE corrections. Values shown in boldface indicate the rate-limiting steps. [b]BSSE corrections are included for the final reaction products.

Table S12. Relative Energies (kJ/mol) of the Reactants, Transition States, Intermediates and Products for Producing $[Ade+H]^+$ from N1 Protonated $[dAdo+H]^+$ and $[Ado+H]^+$ with a Polarizable Continuum Model.

CID Channel		Relative Energies[a]		CID Channel		Relative Energies[a]	
		B3LYP	MP2			B3LYP	MP2
$[Ade+H]^+$	$[dAdo+H]^+$	**0.0**	**0.0**	$[Ade+H]^+$	$[Ado+H]^+$	0.0	0.0
	TS_1	116.0	151.2		TS_1	140.4	174.1
	Int_1	115.9	151.0		Int_1	136.9	172.9
	TS_2	**117.2**	**155.7**		TS_2	**145.1**	**182.3**
	Int_2	42.1	74.6		Int_2	41.1	74.3
	ΔH_{rxn} [b]	33.1	49.5		ΔH_{rxn} [b]	30.4	51.0

[a]B3LYP/6-311+G(2d,2p) and MP2/6-311+G(2d,2p) relative energies of B3LYP/6-311+G(d,p) optimized structures at 0 K including ZPE corrections. Values shown in boldface indicate the rate-limiting steps. [b]BSSE corrections are included for the final reaction products.

Figure Captions

Figure S1. Calculated potential energy surfaces for N-glycosidic bond cleavage of N1 protonated $[dAdo+H]^+$ to produce $[Ade+H]^+$ and $[dAdo\text{-}Ade+H]^+$, parts a and b, respectively. Structures were optimized at the B3LYP/6-311+G(d,p) level of theory. The B3LYP/6-311+G(2d,2p) (shown in blue) and the MP2(full)/6-311+G(2d,2p) (shown in red) relative energies at 0 K are also shown.

Figure S2. Calculated potential energy surfaces for N-glycosidic bond cleavage of N1 protonated $[Ado+H]^+$ to produce $[Ade+H]^+$ and $[Ado\text{-}Ade+H]^+$, parts a and b, respectively. Structures were optimized at the B3LYP/6-311+G(d,p) level of theory. The B3LYP/6-311+G(2d,2p) (shown in blue) and the MP2(full)/6-311+G(2d,2p) (shown in red) relative energies at 0 K are also shown.

Figure S3. Theoretical versus experimental 0 K activation energies (AEs) and reaction enthalpies (ΔH_{rxn}s) for N-glycosidic bond cleavage of N1 protonated $[dAdo+H]^+$ and $[Ado+H]^+$. All values are taken from Table S8.

Figure S4. TS structures along the PESs for N-glycosidic bond cleavage of N3 protonated $[dAdo+H]^+$ and $[Ado+H]^+$.

Figure S5. TS structures along the PESs for N-glycosidic bond cleavage of N1 protonated $[dAdo+H]^+$ and $[Ado+H]^+$.

Figure S1.

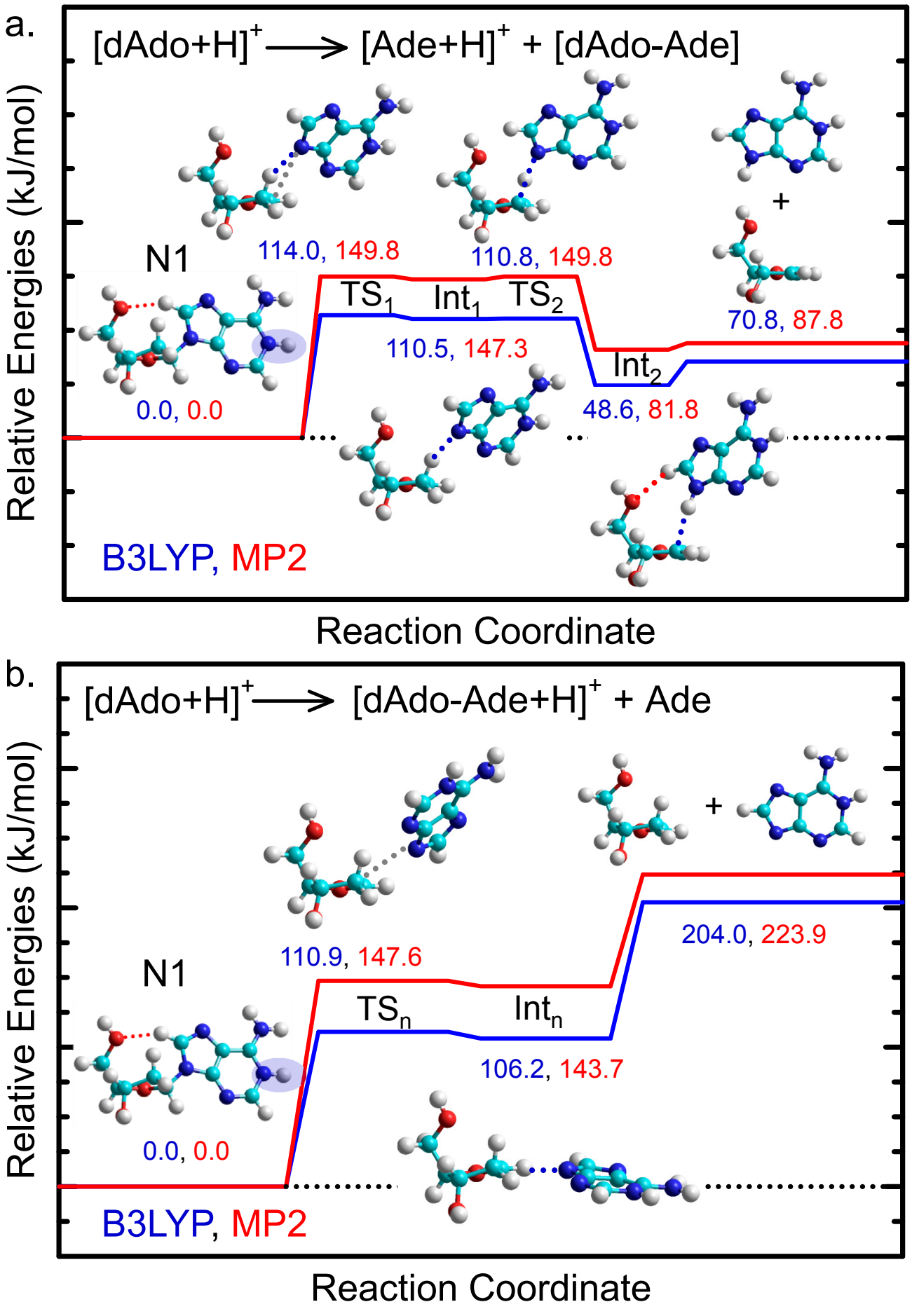
a.
[dAdo+H]+ ⟶ [Ade+H]+ + [dAdo-Ade]
Relative Energies (kJ/mol)
N1
114.0, 149.8
110.8, 149.8
TS1
Int1
TS2
110.5, 147.3
70.8, 87.8
Int2
48.6, 81.8
0.0, 0.0
B3LYP, MP2
Reaction Coordinate
b.
[dAdo+H]+ ⟶ [dAdo-Ade+H]+ + Ade
Relative Energies (kJ/mol)
N1
110.9, 147.6
204.0, 223.9
TSn
Intn
106.2, 143.7
0.0, 0.0
B3LYP, MP2
Reaction Coordinate

Figure S2.

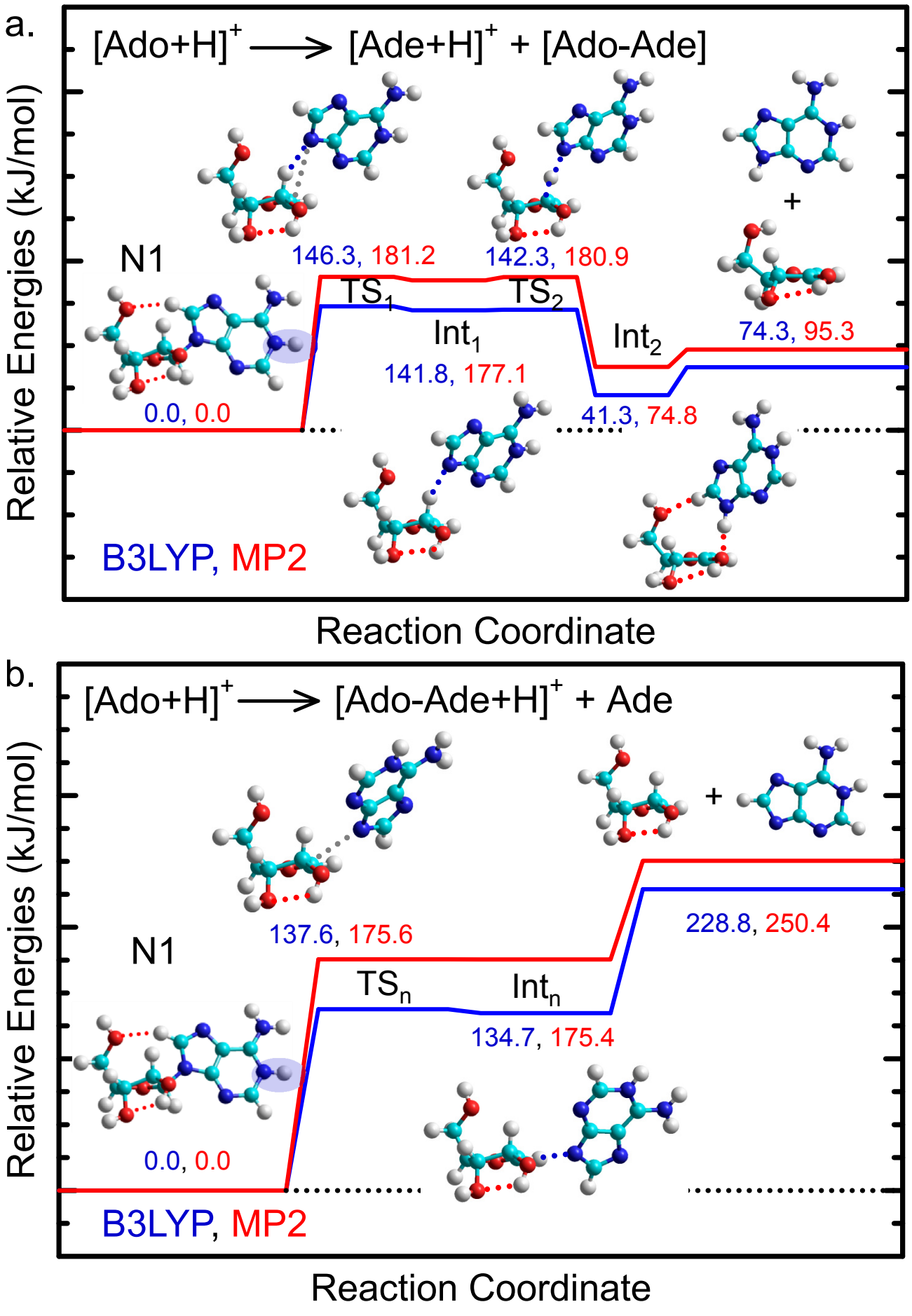
a.
[Ado+H]+ ⟶ [Ade+H]+ + [Ado-Ade]
N1
146.3, 181.2
142.3, 180.9
TS1
TS2
Int1
Int2
74.3, 95.3
141.8, 177.1
0.0, 0.0
41.3, 74.8
B3LYP, MP2
Relative Energies (kJ/mol)
Reaction Coordinate
b.
[Ado+H]+ ⟶ [Ado-Ade+H]+ + Ade
137.6, 175.6
228.8, 250.4
N1
TSn
Intn
134.7, 175.4
0.0, 0.0
B3LYP, MP2
Relative Energies (kJ/mol)
Reaction Coordinate

Figure S3.

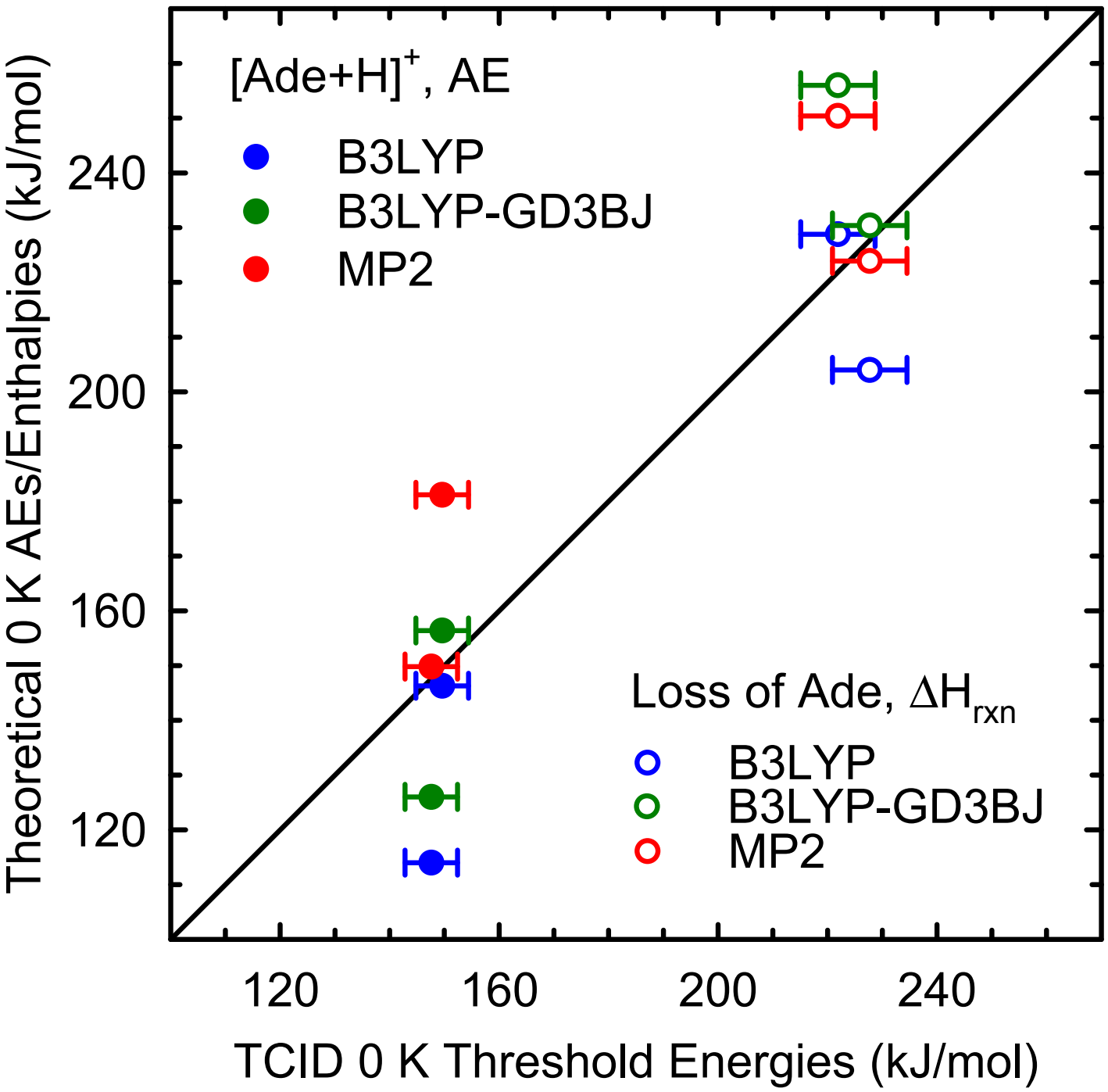
[Ade+H]+, AE
B3LYP
B3LYP-GD3BJ
MP2
Loss of Ade, ΔHrxn
B3LYP
B3LYP-GD3BJ
MP2
Theoretical 0 K AEs/Enthalpies (kJ/mol)
TCID 0 K Threshold Energies (kJ/mol)
120
160
200
240

Figure S4.

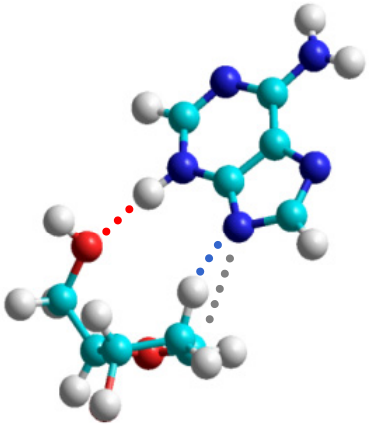

TS_1 146.8, 189.1

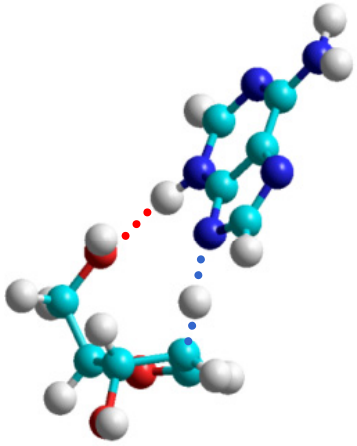

TS_2 136.4, 176.5

N3 $[dAdo+H]^+$ B3LYP, MP2

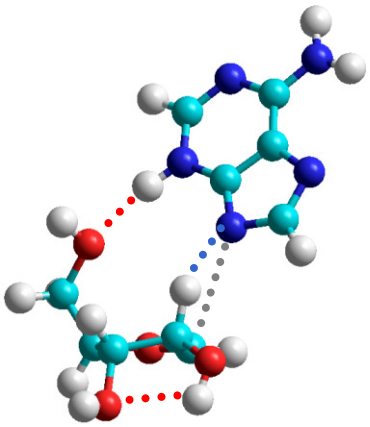

TS_1 172.3, 216.6

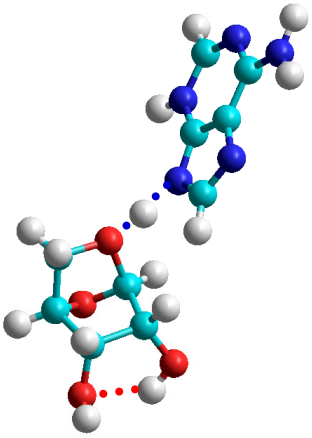

TS_2 161.1, 191.8

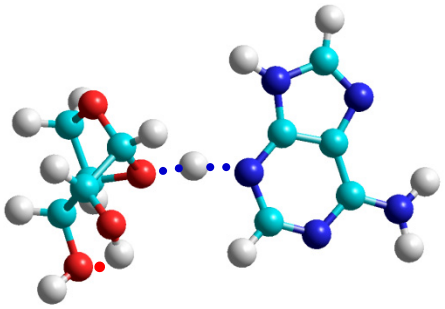

TS_n 155.1, 185.0

N3 $[Ado+H]^+$ B3LYP, MP2

Figure S5.

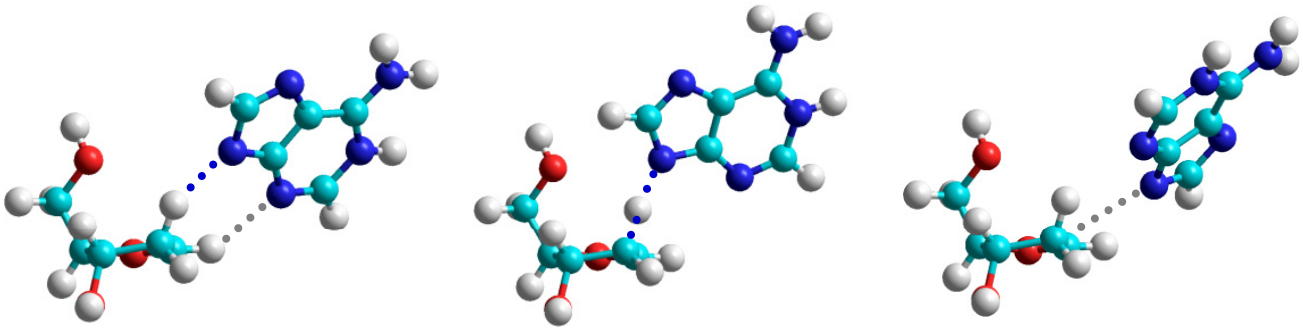

TS_1 114.0, 149.8 TS_2 110.8, 149.8 TS_n 110.9, 147.6

N1 $[dAdo+H]^+$ B3LYP, MP2

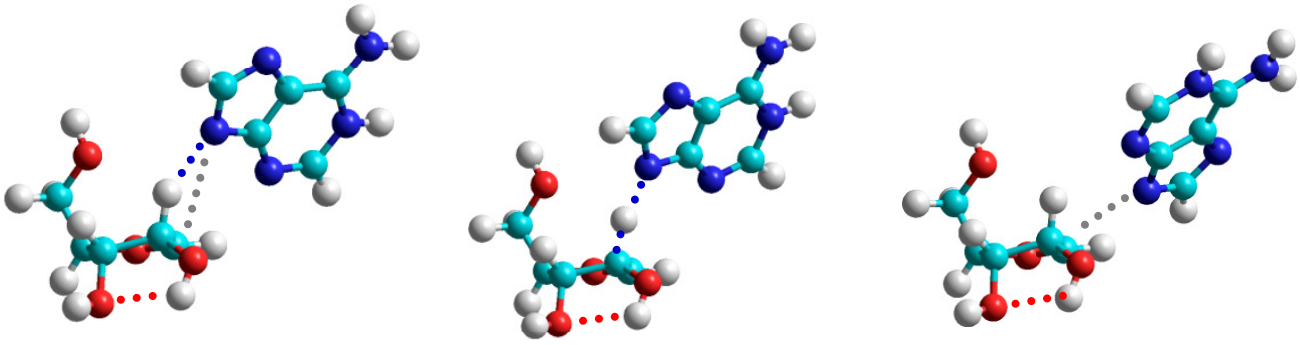

TS_1 146.3, 181.2 TS_2 142.3, 180.9 TS_n 137.6, 175.6

N1 $[Ado+H]^+$ B3LYP, MP2